Journal of Applied Polymer Science

Nanomechanical study of polymer-polymer thin film interface under applied service conditions

G. Mallikarjunachari, Pijush Ghosh
Department of Applied Mechanics, Indian Institute of Technology Madras, Chennai, Tamil Nadu, India
Correspondence to: P. Ghosh (E-mail: pijush@iitm.ac.in or pijushghoshindia@gmail.com)

ABSTRACT: Single layer and multilayer polymer thin film coating on polymer substrate are gaining significant importance in different industries. The quantitative and qualitative estimation of interface response for thin film coating under different service conditions is significantly important from the perspective of modeling and designing novel materials. However, to characterize an interface between the soft polymer layer and soft polymer substrate is challenging because of the confinement effect, surface roughness, the viscoelastic nature of the polymers involved, and most importantly, the comparable mechanical properties of soft polymeric film and polymer substrate. Nanoindentation technique was applied in this work to find out the mechanical response of thin film PMMA (100–200 nm) and Epoxy interfaces of different interfacial strengths. Interfaces of different strengths were obtained by exposing the film-substrate system to different service conditions. It has been observed from this study that pile-up plays a major role in finding out the mechanical response of the interfaces of different strengths. The hardness was observed to increase as the interfacial strength reduces. © 2016 Wiley Periodicals, Inc. J. Appl. Polym. Sci. **2016**, *133*, 43532.

KEYWORDS: coatings; films; mechanical properties; nanostructured polymers

Received 26 August 2015; accepted 9 February 2016
DOI: 10.1002/app.43532

INTRODUCTION

Thin films are often being used in wide varieties of engineering, electronic, optical, and data storage applications. Tissue regeneration, implants, stents, as well as drug delivery are some of the emerging biomedical applications of thin films. Depending on the application, the film thickness varies from several nanometers to several micrometres. In practice, these coatings are often subjected to various types of service conditions such as temperature, pH, and mechanical loading.[1] Recently, ultra-thin polymer coatings (<200 nm) on polymeric substrates are finding substantial industrial applications in the form of multilayer capacitors, organic touch panels, flexible electronics, biomedical, and food packaging. The performance of a polymer-polymer (soft-soft) coating significantly depends on the integrity of an interface since interface failure can potentially lead to the failure of a system. A polymer-polymer interface is developed with contributions from several factors such as physical bonds (van der Waals, hydrogen bond), chemical bonds (covalent bonds), mechanical interlocking, and irreversible plastic heat dissipation.[2] The interface determines the strength of a coating system. Therefore, it is important to evaluate the performance of an interface under various service conditions such as mechanical loading, humidity, and temperature depending on different applications. The repetitive use of these service conditions gradually leads to weakening of an interface. With the weakening of an interface, a critical value of interfacial strength is reached, beyond which, the strength of a coating system gets seriously affected. A mechanical model based on either continuum theory or micromechanics can be developed for a coating-substrate system, which can help predict its performance. The success of a model of this kind in estimating the performance of a system with a significant level of confidence depends on how correctly the properties of these interfaces are determined. Different characterization techniques such as simple tensile fragmentation test, compressive blister test, super layer indentation test,[3] dynamic tests, and contact angle measurements are commonly applied for assessment of thin film interface performance.[4,5] Static and dynamic mechanical characterization of particulate composite materials, coated nanowires, nanofibers surfaces, and interfaces have been also performed.[6–8] However, most of these techniques cannot be efficiently and conveniently applied to characterize polymer-polymer (soft-soft) interface, particularly for ultrathin thickness (<200 nm). Techniques such as depth-

Author Contributions: The manuscript was written through contributions of all authors. All authors have given approval to the final version of the manuscript. All authors contributed equally.

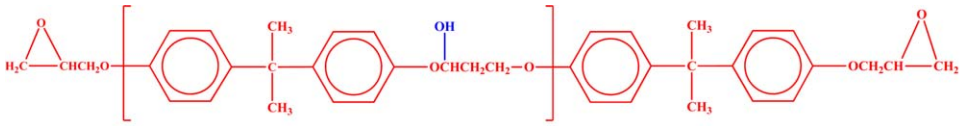

(a) Chemical structure of Diglycidyl Ether of Bisphenol A (DGEBA)

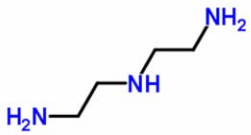

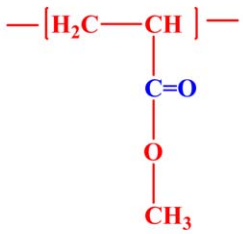

(b) Chemical structure of diethylenetriamine (DETA) (c) Chemical structure of PMMA

Figure 1. Chemical structure of polymers used in this study (a) DGEBA, (b) DETA, and (c) PMMA. [Color figure can be viewed in the online issue, which is available at wileyonlinelibrary.com.]

sensing nanoindentation, nanoscratching,[9,10] and nanoDMA have become more popular in the recent years to evaluate scratch resistance, fracture toughness, dynamic response, and adhesion strength of thin films with high spatial resolution.[11–13] However, determination of mechanical, physical, and thermal properties of ultra-thin polymer films are extremely challenging. This is primarily because of its confinement dependent properties,[14] surface effects (surface roughness)[15] and adhesion effects during indentation,[16] surface pretreatment, alteration of inherent material property during film synthesis, inconvenience of sample handling, substrate effects,[17–20] plastic zone developed under the influence of substrate,[21,22] strain rate sensitivity,[23] comparable properties of film and substrate etc. Apart from above mentioned parameters, pile-up is another important parameter, which makes the soft–soft interface characterization difficult. Pile-up is defined as the accumulation of material above the surface level and around the indenter tip during nanoindentation.[24]

Application of nanomechanical characterization in the past includes the investigation of adhesion strength of soft coating (Teflon) on a hard substrate (TEOS) by Koumoulos *et al.*,[25] interfacial toughness measurement by Gerberich *et al.*[26] They have not reported any film buckling from the surface morphology of the film at the indented region following nanoindentation test. Barletta *et al.* investigated the scratch resistance and adhesion of single layer and multilayer powder coatings on metal and nonmetal substrates.[27–30] The effect of soft substrate on the hard coating and the mechanism of film deformation were established by applying nanoindentation, nanoscratching, and nano-DMA in the past.[31]

As observed in the literature, most of the interface characterization performed applying nanomechanical characterization techniques (mainly scratching) includes either a hard coating or a hard substrate. It is relatively more complex and challenging to characterize an interface built of both polymer substrate and polymer film (i.e., soft-soft interface). The comparable mechanical properties (E, H, and σ_u) and viscoelastic properties such as strain hardening, pile up etc. are the major causes making this characterization challenging. The deformation of substrate together with coating on application of test load, size effect,[32] pile-up contribution from both film and substrate, anisotropy,[33] different loading rate response of film and substrate and the substrate effect on film are some of the practical issues which make a characterization of polymer-polymer interface unique.[34] These are also the major reasons for the absence of any experimental standards and guidelines for performing such characterizations.

In this research, an ultrathin polymer coating on polymer substrate was subjected to a mechanical repetitive loading of increasing frequency to obtain interfaces of different interfacial strengths. Following this, the interfaces were characterized applying depth-sensing nanoindentation techniques.

In a brief, polymer–polymer interfaces of different interfacial strength were characterized applying depth-sensing nanoindentation technique. Besides complementing in modeling and developing design parameters, nanomechanical characterization study of this nature is useful in developing a correlation between interfacial strength and functional efficiency of a thin film in a coating system.

MATERIALS AND METHODS

Thin Film Preparation

The Polymethyl Methacrylate (PMMA) thin film of 150 nm thickness was deposited on Epoxy substrates by spin coating technique. The film thickness was measured using JA Woollam spectroscopic ellipsometer at temperature 18 °C and RH 40%. PMMA (Molecular Weight = 990,000), Diglycidyl Ether of Bisphenol A (Epoxy or DGEBA; Molecular Weight 340.41 g/mol and Diethylenetriamine (DETA; Molecular Weight 103.17 g/mol) supplied by Sigma-Aldrich were used for all experiments.

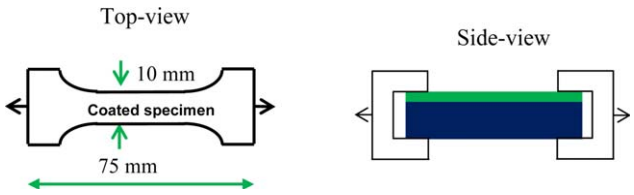

Figure 2. Schematic diagram showing specimen preparation and repetitive loading procedure. [Color figure can be viewed in the online issue, which is available at wileyonlinelibrary.com.]

The chemical structure of DEGBA, DETA, and PMMA are given in Figure 1(a–c), respectively.

Preparation of PMMA Thin Film Coatings Having Different Interfacial Strength

The details of PMMA coated specimen schematically shown in Figure 2. The sinusoidal cyclic load varied from 0.9 to 1 kN. The experimental details for three types of samples are summarized in Table I. Because of this repetitive loading, the interfacial strength between PMMA coating and epoxy substrate decreases with increase in the number of cycles. Thus, sample S_0, S_1, and S_2 are expected to have interfacial strength in the decreasing order with S_0 being one which was not subjected to any loading.

Nanoindentation

Before performing indentation, the surface roughness of the films was characterized applying Scanning Probe Microscopy. The surface roughness is the one the factor that can affect the mechanical properties of thin films during indentation. In general, the surface roughness of semiconductor devices is ~1 nm. However, the surface roughness of engineering films varies from 100 nm to 1 μm. The RMS roughness of the surface obtained was 05 nm, which was small enough to affect the measurement of mechanical properties.[35] The quasi-static nanoindentation experiments were carried out using Hysitron TI 950 instrument with the Berkovich tip (radius ~150 nm and half angles of 65.35°) made of diamond (Young's modulus $E = 1140$ GPa, Poisson's ratio $v = 0.07$). The indentation tests were carried out at an ambient temperature of 17 °C and at a relative humidity of 45%. As load increases, the residual area of indentation increases (because of larger stress influence region). To avoid the overlapping or influence of one indentation on other, the number of indents over a given area were adjusted accordingly. Appropriate load function (loading 20 s, holding 10 s, and unloading 10 s) was used for all the samples. All tests were repeated 15–20 times. The hardness H and Young's modulus E were obtained as a function of load (or penetration depth) given by eq. 1 and were directly obtained from the instrument.

$$H = \frac{P}{A_c} \ldots (i)\ A_c = f(h_c) = C_1 h_c^2 + C_2 h_c + C_3 h_c^{1/2} + C_4 h_c^{1/4}{}_r \ldots (ii)\ E_r = \frac{\sqrt{\pi}}{2\beta}\frac{s}{\sqrt{A_c}} \ldots (iii) \quad (1)$$

where, P is the maximum load, C_1, C_2, C_3, C_4, and β are the constants and E_r is the reduced Young's modulus as expressed in eq. (1-*iii*).

RESULTS AND DISCUSSION

Thin Film Surface Morphology Characterization

Two test samples were subjected to mechanical service (loading) conditions (S_1 and S_2) as explained in the experiment section. The sample S_0 was not subjected to any loading as indicated in Table I. When a substrate-coating system is subjected to cyclic repetitive loading, the shear stress developed weakens a film-substrate interface. With the increase in the number of cycles, more shear stress at the interface causes further weakening of an interface. A schematic representation of interfaces of three different adhesion strengths is shown in Figure 3. The white area around the interface is proportional to the loss in strength suffered caused by service conditions. This weakening of interface was reflected through the propagation of cracks to the surface as shown in Figure 4(a–c). It is expected that interface damage first since the interface is the weakest zone compared to individual properties of film and substrate. The intensity of cracks is the direct representation of damage at the interface because of delocalization of strain.[36,37] The inset shows the enlarged view of crack developed after service loads S_1 and S_2 were applied. The increasing deterioration or weakening of interfaces of S_2 compared with S_1 was confirmed by optical images and SEM images either through crack intensity or cracks per unit area or both.

The effect of increasing service load on coating (150 nm)—the substrate interface was analyzed following indentation at the interfaces. Load-controlled nanoindentation tests were performed on each sample S_0, S_1, and S_2 to determine the response of the interface for each case. Different peak loads starting from 80 to 500 μN were applied in a way that the maximum penetration depth of indentation attained falls in the regions above the interface (P_1), at the interface (P_2) and beneath the interface (P_3) as shown in Figure 5. Before performing tests on S_0, S_1, and S_2 samples, nanoindentation was performed on bulk PMMA and bulk epoxy to get the inherent response of these materials. Standard error was applied for the E and H values.

Young's Modulus

In case of a bulk material, the elastic response during indentation comes from material underlying the indenter as well as from the tip itself. Generally, Young's modulus (E) of a polymer

Table I. Details of Samples (S_0, S_1, S_2) for Nanoindentation

Set	Film thickness (nm)	Film	Substrate	No. of cycles	Frequency (Hz)
S_0	150	PMMA	Epoxy	0	0
S_1	150	PMMA	Epoxy	40,000	15
S_2	150	PMMA	Epoxy	120,000	15

Figure 3. Schematic diagram representing expected damage to the interface as the service load increases. More interface damage is expected in case of S_2 compared with S_1. [Color figure can be viewed in the online issue, which is available at wileyonlinelibrary.com.]

is much lesser when compared with that of a diamond tip and thus the reduced Young's modulus (E_r) can be considered as the representative value of bulk polymer alone. Elastic recovery occurs upon removal of indenter from the surface thus giving measurable unloading elastic contact stiffness. The measured E after pile-up correction for bulk PMMA is 3.9 GPa and for Epoxy is 4.35 GPa. In case of a thin film coating system, however, the elastic response is a combined response of the film, the interface and the substrate involved. The properties of the film, the interface, and the substrate are expected to have major contributions on the modulus determined at shallow (below 10% of film thickness), intermediate (near interface) and larger depth, respectively. It is relatively simple to characterize an interface for a soft coating on a hard substrate applying nanoindentation technique. Large relative differences in the mechanical properties of a soft film and a hard substrate cause a significant jump in E value as an interface is approached. To distinguish between the effects of substrates, nanoindentation tests were also performed on a hard substrate (silicon wafer) and soft coating (PMMA).

The E values obtained on 150 nm PMMA coated film on Silicon wafer are shown in Figure 6(a). With the depth of penetration exceeding 10% of the film thickness, an increase in the E value was observed due to substrate effect. As the penetration depth approaches nearer the interface (130–160 nm), the E values are observed to remain almost constant up to a certain depth. This zone is marked with a dotted circle in the same figure. The E value is found to increase again as the indenter penetrates the si-wafer substrate with an increase in depth. The response within a dotted circle zone is termed as the interface response. This interface response is different depending on a coating-substrate combination such as a soft coating on a hard substrate, hard coating on a hard substrate, hard coating on a soft substrate, etc. This is mainly because the volume of the material enclosed in the elastoplastic and plastic region under the indenter changes depending on the film-substrate combination. Further, the properties of these enclosed materials significantly influence the E values measured.

The response of E values for sample S_0 is noted to be different from the responses obtained for Si- wafer substrate with increasing depth as observed in Figure 6(b). There is no well-defined region in the curve, which can be attributed to the interface. However, an increase in E values observed at depths 100 and 175 nm shown in a dotted circle is not significantly high. One of the possible reasons is the comparable E value of bulk PMMA and bulk epoxy. The E values for three service condition S_0, S_1, and S_2 are shown in Figure 6(b). The E values decrease and then becomes constant with increasing the indentation load for all the three service conditions. Moreover, the E value also decreases with increasing the service condition for a particular indentation load. The reduction in E values is due to the loss in the strength of the interfaces during the service conditions.

Hardness

The indentation hardness is essentially a measure of the plastic deformation of a sample underneath the tip. Different sets of load starting from 40 to 500 μN were applied to measure the hardness of bulk PMMA and bulk epoxy. In general, the value of the mean contact pressure P_m at which there is no increasing indenter load is related to the hardness (H). The hardness values measured for bulk PMMA and epoxy after pile-up correction are 188 and 197 MPa, respectively. Interestingly, it was observed that for all sets of loads, the H values increases as the interfacial strength decreases. The possible mechanisms involved in this response have been discussed in the later sections. For materials such as polymers, hydrogels, cartilages etc., Oliver-Pharr[38] calculations do not allow the accurate estimation of E

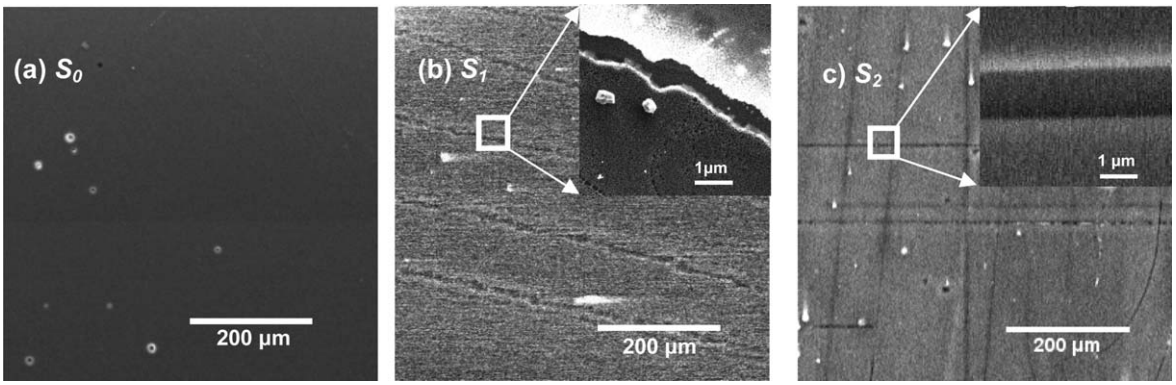

Figure 4. Scanning Electron Microscopy (SEM) images showing surface morphology of three test samples after PMMA/epoxy thin film system subjected to (a) no loading, S_0, and repetitive loading, (b) S_1, and (c) S_2. The inset picture shows the enlarged view of crack developed after applying service load.

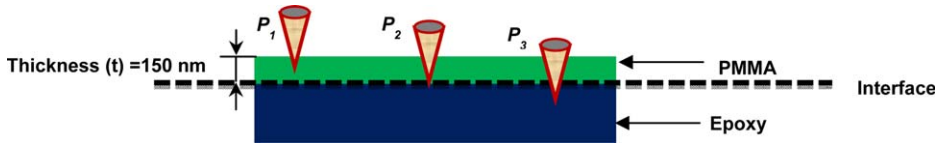

Figure 5. Schematic representation of PMMA and Epoxy layered composite system showing different positions of nanoindenter after reaching the peak load. P_1 represents the load corresponds to indentation above the interface, P_2 at the interface and P_3 below the interface. [Color figure can be viewed in the online issue, which is available at wileyonlinelibrary.com.]

and H values. One of the main reasons behind this inaccuracy in measurement is the pile-up, which affects measured contact area significantly with respect to the one calibrated on standard material. In the presence of a pile-up, the true contact area is underestimated thus resulting in a higher value of H than the actual value. Polymers show pile-up due to lack of work-hardening capacity. The piezo images of the indentations and the measured pile-up on bulk PMMA used for this study at loads 80, 200, and 500 μN are shown in Figure 7(a,b), respectively. These surface pile–up profiles were considered along the section (white line) passing through indentation. They are asymmetric because of the three-sided pyramidal Berkovich indenter tip geometry. It was observed that the height and width of pile-up increase with the increase in indentation load on bulk PMMA. A systematic pile-up study was performed on all these samples S_0, S_1, and S_2 to evaluate the mechanical properties.

Besides Young's modulus, the hardness values were determined for a 150 nm PMMA coated film on a silicon wafer substrate. This was done to understand the response of a soft film on a hard substrate. The varying hardness with increasing depth is shown in Figure 8(a). The increase in the H values was observed for all the depths applied up to a maximum of 180 nm. Unlike E values, as shown in Figure 6(a), no load independent constant region was observed. However, there is a region (as circled), which clearly indicates a slope change.

The depth corresponding to this slope change is approximately the depth of the interface. A significant difference was noticed in the H values measured with an increasing service loads S_0, S_1, and S_2 as shown in Figure 8(b). At any given depth, it was observed that the H values increase as interface gets more damaged (i.e., with repetitive loading). There is not much difference in the H values for sample S_1 and S_2. However, a significant difference in H values was observed between S_0 and S_1 or S_2. This differences increase as the maximum penetration depth of indentation approaches the interface. This zone is represented by dotted lines in the depth range 100–150 nm in the same figure. This is also indicative of the fact that these differences or changes in H are more because of interface weakening than the damage of substrate or film material.

Analysis of Contact Area

Difference between Measured Projected Area and Actual Projected Area. Normally the measured contact (projected) area [A_c from eq. 1] from standard calibration sample (quartz material) holds good for ceramic materials and metallic materials. The contact area is completely different when material exhibits pile-up. The difference in measured contact area (shaded by yellow in color) and actual contact area (shaded by blue in color) is schematically shown in Figure 9. Pile-up not only depends on material intrinsic parameters, it will depend on various extrinsic parameters such as properties of the substrate underlying the indenter, film thickness, rate of loading etc. For example effect of substrate on the thin film, pile-up is illustrated in Figure 10. It was observed PMMA thin film exhibits more pile-up in the case of hard substrate (silicon wafer) when compared to the soft substrate (epoxy) for the same depth

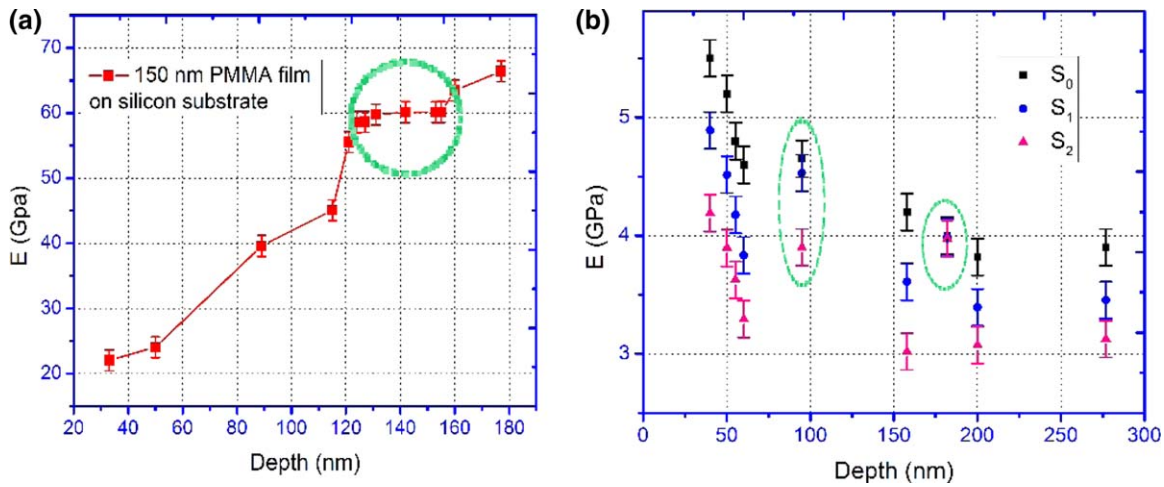

Figure 6. (a) Young's modulus of PMMA coating on Silicon wafer (values within the dotted circle are E values when the tip approached to the interface and are almost constant) and (b) young's modulus of PMMA coating on Epoxy at service conditions. [Color figure can be viewed in the online issue, which is available at wileyonlinelibrary.com.]

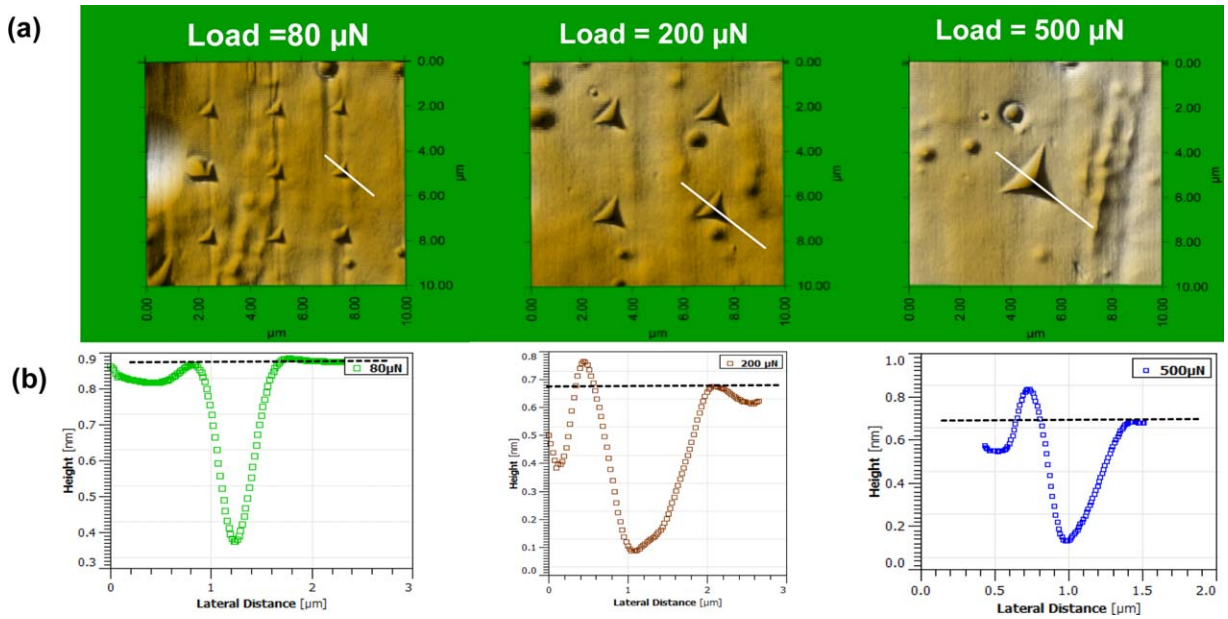

Figure 7. (a) Scanning Probe images corresponding to loads 80, 200, and 500 μN on bulk PMMA (b) Plots showing the pile-up height corresponding to loads 80, 200, and 500 μN along the white line (represented in same Y axis length scale). Observed pile-up increases with the increasing load. [Color figure can be viewed in the online issue, which is available at wileyonlinelibrary.com.]

of penetration (i.e., 300 nm). In this work, the actual projected area (surrounded by a white line) shown in the same figure was calculated from image analysis for all sets of loads and samples.

The H for each sample S_0, S_1, and S_2 (mentioned above) was calculated using the load and the projected contact area measured from piezo images. Image analysis was performed to measure the magnitude of projected area with pile-up at different service conditions S_0, S_1, and S_2. The indentation with load values of 80, 200, and 500 μN were performed near the crack on sample S_0, S_1, and S_2. As mentioned earlier, these loads correspond to indentation position at the film, interface, and substrate respectively. A top-view piezo images of samples S_1 and S_2 for the loads 80, 200, and 500 μN are shown in Figure 11(a,b), respectively. These images also provide a general indication of the intensity of cracks formed on the sample S_1 and S_2 with increasing number of load repetition.

High-resolution 3D piezo image of pile-up observed in case of S_0 is shown in Figure 12(a). The section profiles of indentation applied to compare the height and the width of a pile-up at the same loading of 200 μN for S_0, S_1, and S_2 are shown in Figure 12(b). The ratio of a pile-up corrected area and the area estimated from Oliver–Pharr method for three service conditions S_0, S_1, and S_2 is shown in Figure 12(c). This indicates the decrease in the amount of underestimation during the

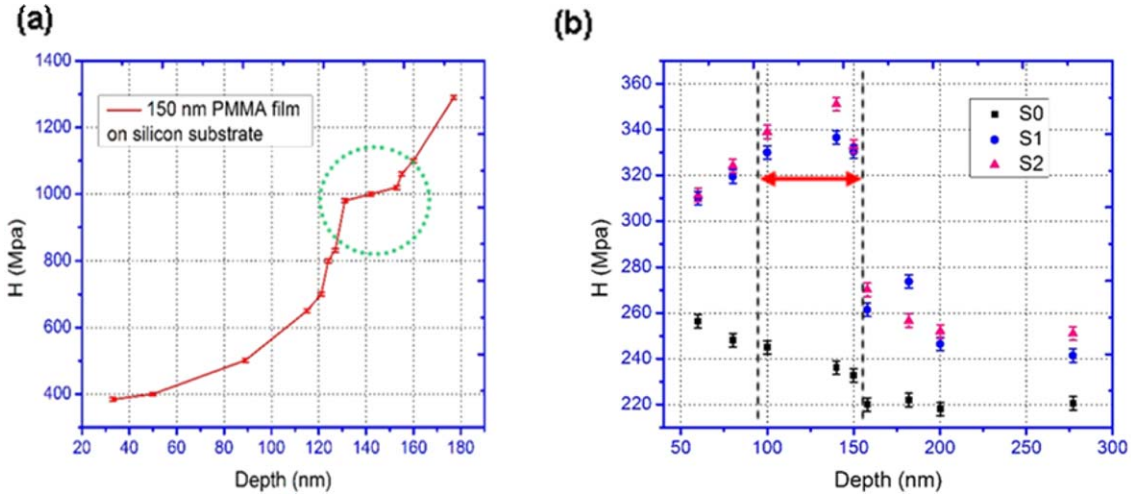

Figure 8. (a) Hardness of PMMA coating on Silicon wafer (values with in the dotted circle are H values when the tip approached to the interface and are almost constant). (b) Hardness of PMMA coating on Epoxy at service conditions S_0, S_1, and S_2. Values in between dotted lines shows H values when the maximum penetration depth approaches the interface. [Color figure can be viewed in the online issue, which is available at wileyonlinelibrary.com.]

Figure 9. Schematic diagram showing difference in contact (projected) area with and without considering pile-up. [Color figure can be viewed in the online issue, which is available at wileyonlinelibrary.com.]

computation of projected area as an interface weakens. Further, it was observed that the amount of pile-up is different for bulk PMMA and for thin film PMMA coated on the epoxy substrate. This difference arises mainly because of the confinement effect of thin film and the substrate effect of epoxy. Scanning probe microscopy was applied to measure the depth and width of the indentation profile and the height of pile-up. It was observed that the height and width of pile-up decrease as the service load increases for all the loads. These differences in the pile-up magnitude were observed due to the weakening of the interface.

The material volume near an indenter tip can be classified primarily into two types. A proportionally small plastic region immediately adjacent to the tip followed by an elastic region, which spreads over a larger diameter. Between these two, however, there is an elastoplastic region, which undergoes property transition and significantly contributes to the pile-up characteristics of a material during indentation. The ability of a material to undergo strain hardening under compression stress path also significantly depends on the characteristics of this elastoplastic region. The shape of this elastic and plastic region can be assumed to be spherical for indentation on bulk material. However, for a coating system, the elastic region can be assumed to be of some irregular shape symmetrical about tip axis as shown in Figure 13(a). The plastic region being proportionally small can still be assumed to be spherical. We believe that the shape and the volume of these elastic and elastoplastic regions change with a change in interface characteristics as indicated in Figure 13(b,c).

In case of sample S_0, where the interface is not damaged, the material bound by the elastic and elastoplastic region is mainly displaced in the upward direction as shown in Figure 13(a). However, with an increase in interface damage the load transfer behavior changes and the possibility of material flow in the lateral direction increases [Figure 13(b)]. With the further increase in damage (S_2), the material tends to flow almost in all directions [Figure 13(c)]. For these three different conditions, the volume component of material undergoing strain-hardening adjacent to the tip is expected to be different. This material flow characteristic for S_0, S_1, and S_2 leads to different magnitudes of pile-up thus resulting in different H values as measured.

Effect of Interface on Maximum Penetration Depth

Besides E and H values, another important parameter, which can provide insight into the interfacial strength, is the maximum penetration depth at a given load. The maximum penetration depth as a function of load for bulk PMMA, bulk epoxy, and PMMA/Epoxy film at different service conditions (S_0, S_1, and S_2) is shown in Figure 14. It was observed that in case of bulk PMMA and bulk epoxy, the maximum penetration depth varies approximately linearly with increasing load as shown in Figure 14(a). However, in case of a PMMA/Epoxy film (S_0), the

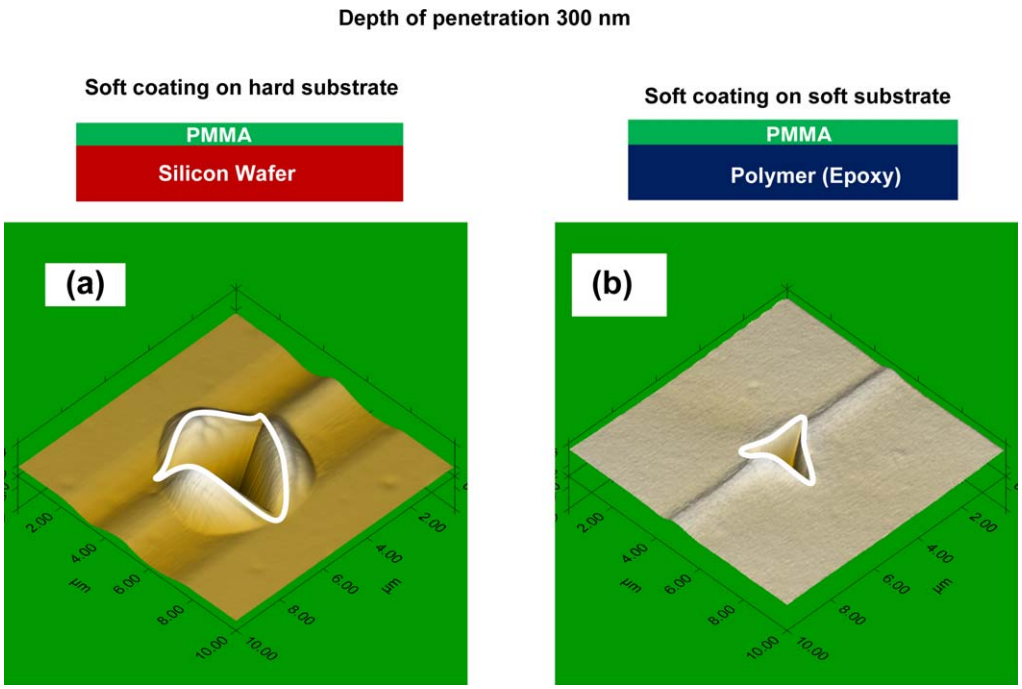

Figure 10. Piezo images showing pile-up obtained after nanoindentation at depth of penetration 300 nm. (a) 150 nm film on silicon wafer. (b) 150 nm film on epoxy substrate (area surrounded by white line is actual area measured by considering the pile-up). [Color figure can be viewed in the online issue, which is available at wileyonlinelibrary.com.]

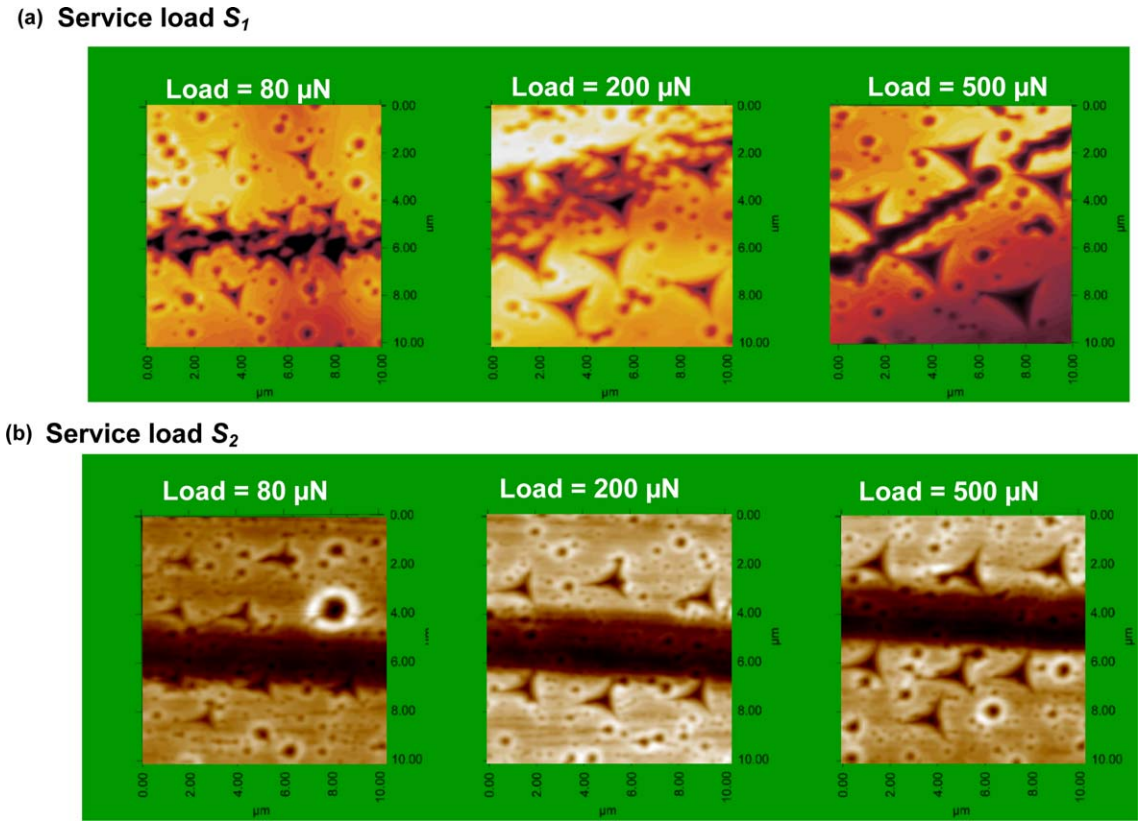

Figure 11. SPM image of PMMA/Epoxy coated specimen at loads 80, 200, and 500 μN for service loads (a) S_1 and (b) S_2. Images showing the indentation residual impressions near the crack. [Color figure can be viewed in the online issue, which is available at wileyonlinelibrary.com.]

slope was found to vary with indentation depth. As observed in Figure 14(b), at point A, the load displacement curve undergoes a significant change in the slope. The depth corresponding to point A is approximately the depth of the interface or the thickness of the PMMA film. Following this region A, the slope remains almost constant, indicating that the indenter has crossed the interface and entered into the epoxy substrate.

The slope of this characteristic curve is considered as an indicator of the relative stiffness of the film and substrate material. The spread of region II can provide significant insight into the thickness of the interface of a coated system. The loads versus maximum depth of penetration for coated sample subjected to service condition S_0, S_1, and S_2, are compared as shown in Figure 14(c).

The slope of a tangent drawn at point A to the respective curves is designated as $\tan(\theta_0)$, $\tan(\theta_1)$, and $\tan(\theta_2)$ for S_0, S_1, and S_2, respectively. It was observed that $\tan(\theta_0) > \tan(\theta_1) > \tan(\theta_2)$. This indicates that loss in strength of interface due to service condition leads to larger penetration of indenter tip around the interface region for any given load. The nature of the curve in Region I and Region III is almost linear. However, in Region II, it is expected to be nonlinear. The degree of nonlinearity

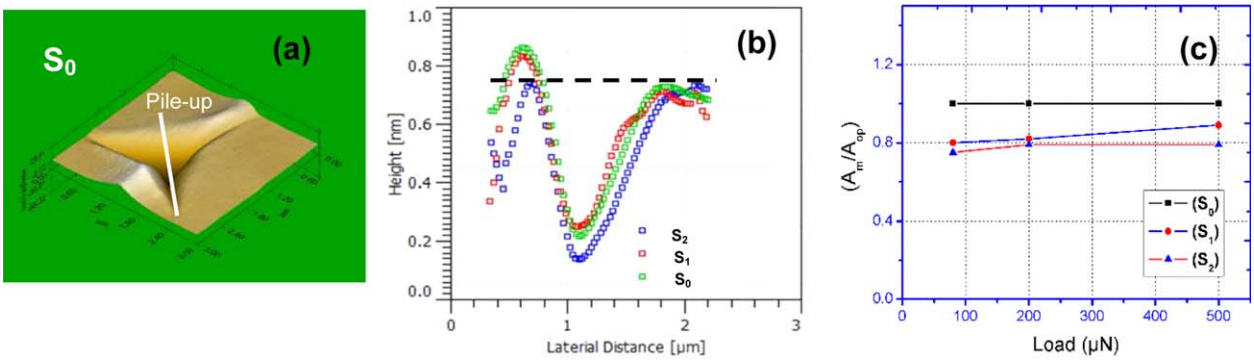

Figure 12. (a) High resolution 3D image showing pile-up for 150 nm PMMA/epoxy system at S_0, (b) Observed pile-up for S_0, S_1, and S_2, pile-up decreases as the interface weakens, and (c) ratio of pile-up corrected area to area obtained from Oliver-Pharr method. [Color figure can be viewed in the online issue, which is available at wileyonlinelibrary.com.]

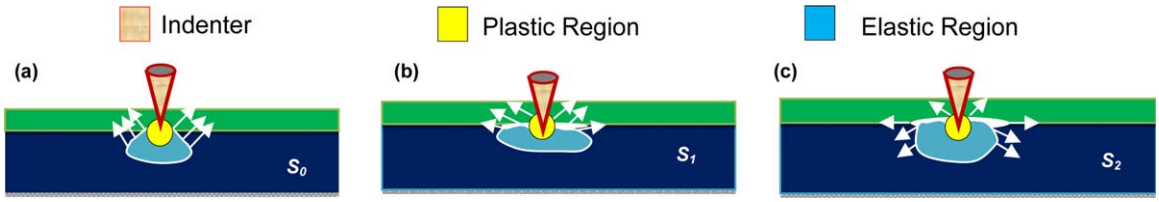

Figure 13. Schematic diagram showing elastic region, plastic region under indenter tip and the possible direction of material flow for the same load at different service conditions. (a) S_0: material flow in upward direction and (b) S_1: material flow in lateral direction, and (c) S_2: material flow in almost all directions. [Color figure can be viewed in the online issue, which is available at wileyonlinelibrary.com.]

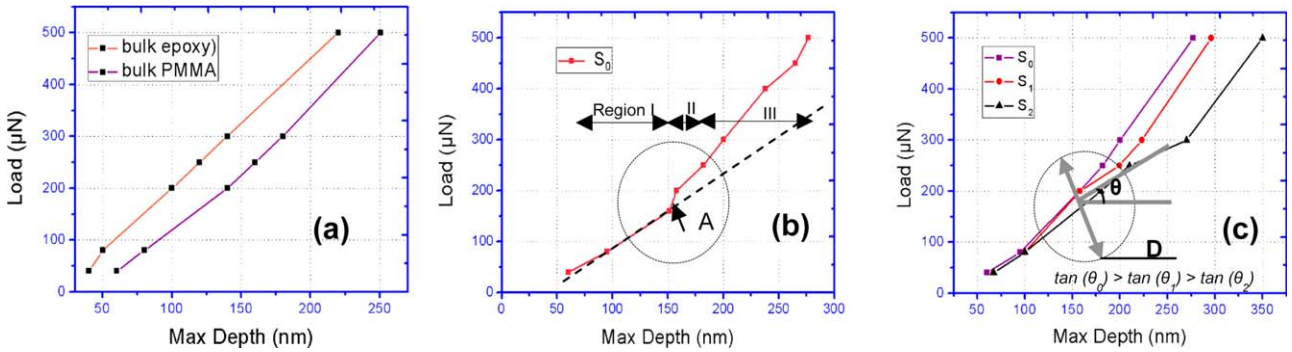

Figure 14. The load versus maximum penetration depth curves obtained from experiments. (a) Bulk PMMA and bulk epoxy (slope of the curve is approximately linear). (b) S_0: slope deviation at point A, that is, maximum penetration depth approaches nearer the interface (the dotted line is added as a reference straight to show the slope change of the curve S_0). (c) Deviation in the load versus maximum penetration curves for S_0, S_1, and S_2. [Color figure can be viewed in the online issue, which is available at wileyonlinelibrary.com.]

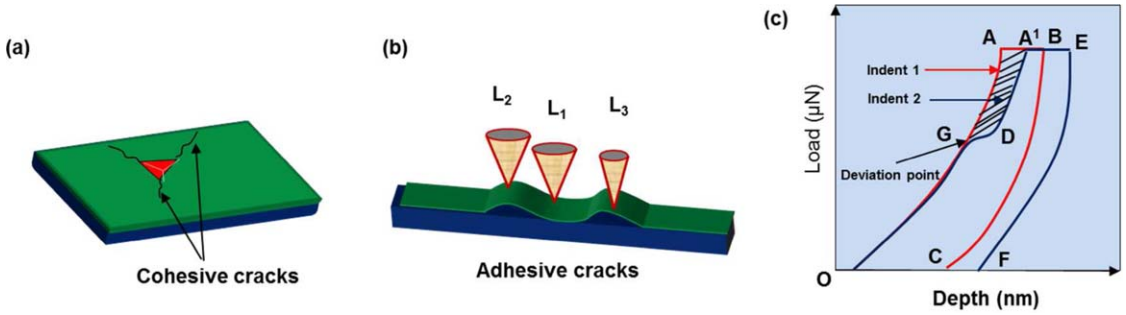

Figure 15. Schematic diagram showing different possible cracks during indentation (a) cohesive cracks generated on surface of the film at the critical load. (b) Adhesive cracks (double buckling) at the interface at higher penetration depth. (c) Observable feature (slope change) at point "G" on a load – displacement plot in a nanoindentation test. [Color figure can be viewed in the online issue, which is available at wileyonlinelibrary.com.]

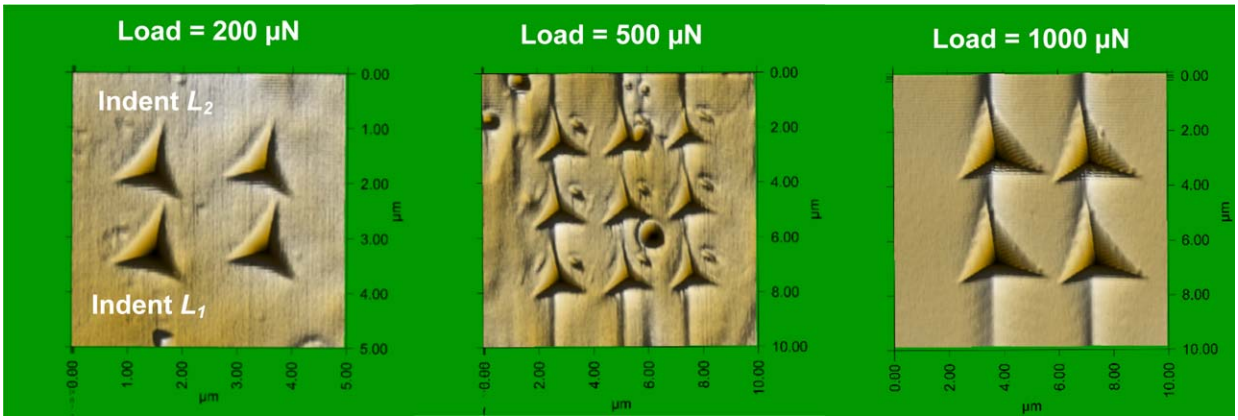

Figure 16. Piezo images showing indentations nearer to each other for loads 200, 500, and 1000 μN (surface morphology confirms no cohesive cracks developed as the load increases up to 1000 μN). [Color figure can be viewed in the online issue, which is available at wileyonlinelibrary.com.]

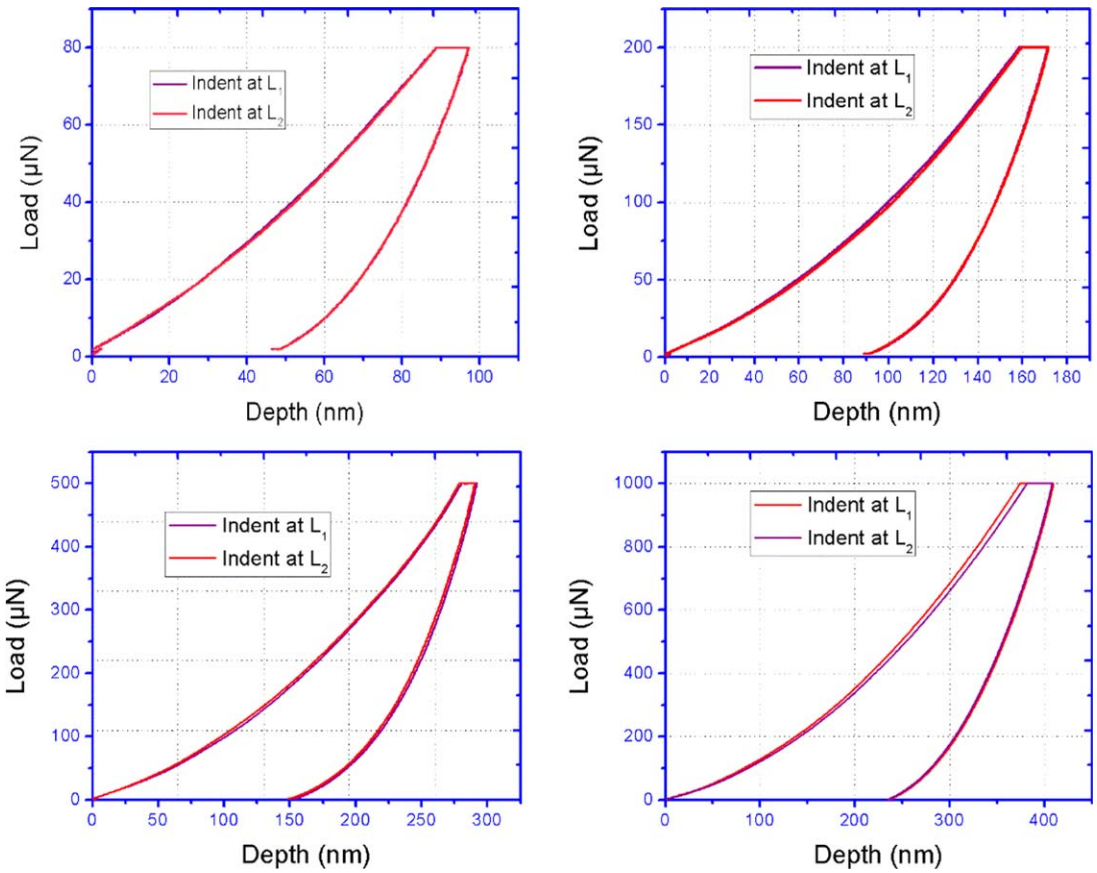

Figure 17. Load displacement plots on two adjacent points (L_1 and L_2) for different loads of 80, 200, 500, and 1000 μN, respectively. The load-displacement curves at two points are almost overlapping each other at any given load. [Color figure can be viewed in the online issue, which is available at wileyonlinelibrary.com.]

depends on the interface adhesion strength and nature of loading. The two parameters obtained from this characteristic curve, the slope θ and diameter "D" of region II, can provide significant information during modeling of a coating as a three phase system (substrate-interface-film). The stiffness can be approximately estimated from the θ value. The thickness of interface or an interface volume as a percentage of substrate volume can be obtained approximately from the diameter "D" of the region II. To develop a complete model using this information, more experiments are necessary to be done with different combinations and multiple repetition, which is beyond the scope of this work. It is therefore observed that for a coated system, the loss in interfacial strength incurred on being exposed to different service conditions can be quantitatively characterized by depth-sensing nanoindentation technique. Any viscoelastic model developed to characterize a coating system would, however, need nano-DMA studies at the interface to more accurately predict and determine the necessary parameters.

Energy Analysis

Indentation on a thin film coating system can lead to following two possible phenomena.

i. Cohesive cracks in the form of channels, propagating radially outward from the point of indent as shown schematically in Figure 15(a). The extent of cohesive cracks depends on the nature of both substrate and film material such as brittleness, ductility etc.
ii. Adhesive cracks (delamination or buckle) adjacent to the indenter could be a single buckle or double buckle as shown in Figure 15(b). This buckling mainly depends on the type and shape of the indenter, the amount of load, penetration depth, and relative stiffness of the film and substrate.

The presence of any of the above two cracks can result in a load-displacement response which is different from a one without cracks. The strain energy released during the process of cohesive or adhesive cracks can be approximately calculated from the typical response feature such as steps as shown schematically in Figure 15(c). Here, OGABCO is the area under the curve obtained in the ideal case, and ODA^{1}EFO is the area under the curve obtained due to cohesive or adhesive crack development. The area under the curve AA^{1}DGA (shaded region) represents the energy difference which is released as strain energy due to the formation of cohesive or adhesive cracks.

To find out the development of buckling next to the indenter, indentations on the immediate neighborhood L_2 and L_3 were performed as shown in Figure 15(b). Should there be any delamination, the load-displacement response at positions L_2 and L_3 will be different from L_1 with additional features such as

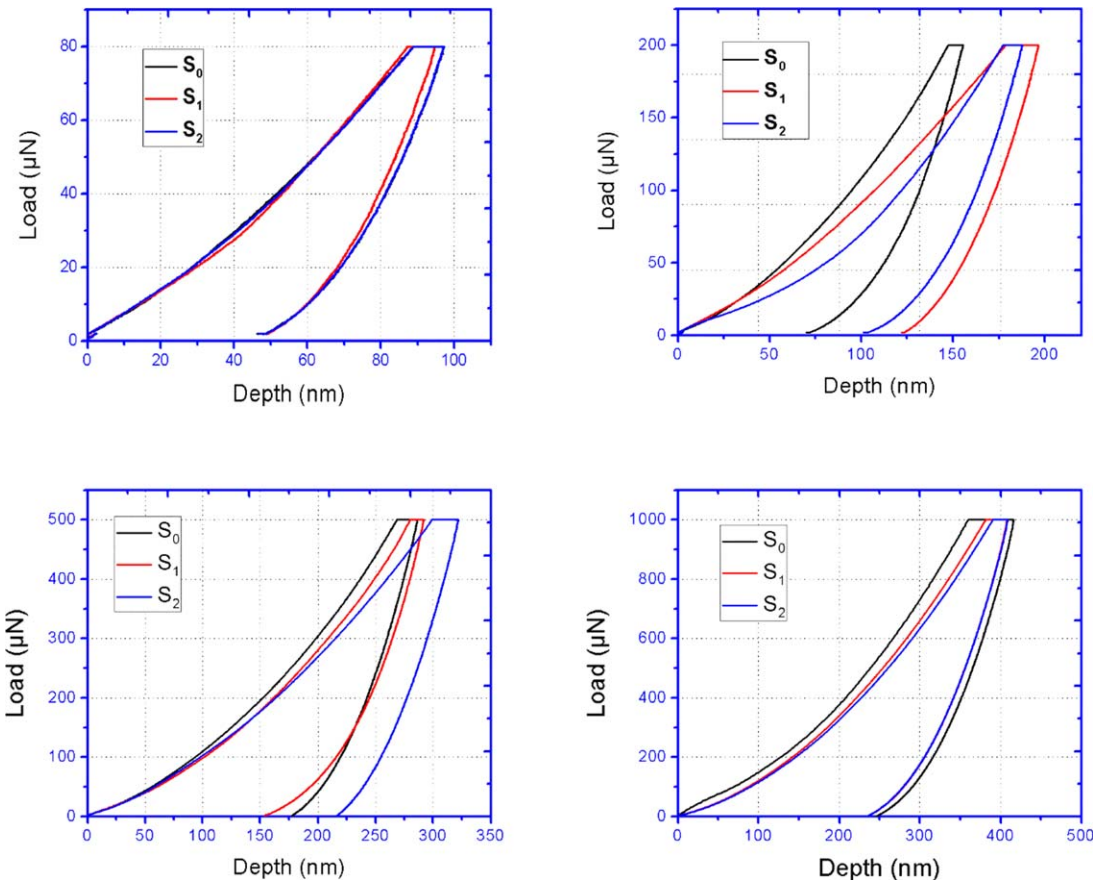

Figure 18. Load displacement plots showing deviations in loading and unloading segments for loads 80, 200, 500, and 1000 μN (the deviation in the load-displacement curve is more for the load 200 μN). [Color figure can be viewed in the online issue, which is available at wileyonlinelibrary.com.]

steps, pop-ins, and pop-ups. In addition, due to indentation, the plastic region under the indenter at L_1 can extend laterally to the immediate neighborhood of L_2 and L_3. This can thus transform the material to behave more plastic at L_2 and L_3. The mechanical characterization of this new material property can also be determined by performing indentation at L_2 and L_3.

We have performed a detailed analysis (explained below) to find out if any cohesive or adhesive cracks mentioned above developed for gradually increasing the load on sample S_0. Further, this analysis was applied on samples S_1 and S_2 to determine the development of delamination, if any, due to service loading alone. SPM images after indentation on S_0 sample (150 nm PMMA-Epoxy system) at three different loads 200, 500, and 1000 μN are shown in Figure 16. There are no cohesive cracks seen even for the load as higher 1000 μN.

One of the possible reasons for the cohesive and adhesive cracks to not appear in a soft-soft system is the relative values of E and H of the film (PMMA) and substrate (epoxy). As a result of this, a significant part of the externally applied energy in the form of indenter load is absorbed in the deformation of the film as well as the substrate, thus making sufficient energy unavailable for the formation of cohesive and adhesive cracks. Nanoindentation load-displacement plots on S_0 sample for loads 80, 200, 500, and 1000 μN are shown in Figure 17. Since load-displacement plot of indent at L_1 and L_2 is almost overlapping exactly for all loads, it can be inferred that the plastic region under indenter at L_1 has not extended laterally enough in the immediate neighborhood. Thus, the possibility of any such buckling phenomenon next to the indenter is also very unlikely for sample S_0 within the applied load range.

However, the nature of the load-displacement curve (response) of S_1 and S_2 when compared to S_0, show the significant difference as indicated in Figure 18. The transition behavior, maximum penetration depths, and energy differences as observed for S_1 and S_2 can be attributed to the weakening of the interface due to service load. The work of indentation, elastic energy, and plastic energy for three conditions at 200 μN are mentioned in Table II.

Table II. Work of Indentation, Elastic Energy, and Plastic Energy for Interfacial Strength at 200 μN

Service condition	Total work of indentation ($10^{-15} \times$ J)	Elastic energy ($10^{-15} \times$ J)	Plastic energy ($10^{-15} \times$ J)
S_0	14957	5940.12	9016.18
S_1	15015.21	5827.31	9187.9
S_2	16079.14	4894.78	11184.36

It was observed that the plastic energy dissipation increases, whereas, the elastic energy recovery decreases as the interface weakens. This energy dissipation and elastic recovery are clearly reflected in the hardness and Young's modulus values as determined previously. A weak interface facilitates the dissipation of plastic energy. In this way, it can be mentioned that as the interface weakens, the damage caused by indentation becomes more irrecoverable.

The magnitude of this plastic energy dissipation depends on the nature of the substrate-film combination (soft-hard, hard-soft, soft-soft etc.). More interestingly, for soft-soft combination, as observed, it depends on the magnitude and rate of loading. The selection of applied load to capture the differences of energy dissipation due to different interfacial strength is important as evident from Figure 18.

CONCLUSIONS

Depth sensing nanoindentation was applied to characterize thin film PMMA coated Epoxy interface of different interfacial strengths. Interfaces of different strengths were developed by exposing the interfaces to service conditions of mechanical repetitive loading for increasing number of cycles. Pile-up corrected E and H values of bulk and coating PMMA was determined at different loads. The modulus value E was observed to decrease with decreasing interfacial strength for all loads. The hardness, however, was observed to increase as interface gets weakened. The pile-up characteristic was found to be the primary reason for the differences in the hardness values observed. The differences in hardness values between a normal interface (S_0) and weak interfaces (S_1, S_2) observed to be more near the interface. The response of an interface was observed to be different depending on whether PMMA is coated on a soft substrate (epoxy) or a hard substrate (silicon wafer). The quantity of plastic energy dissipation was observed to increase as the interface becomes weaker. The load-displacement response near the interface was observed to be nonlinear in nature and this response can be applied to estimate the thickness of an interface. This study is helpful in interface design and modelling of a soft polymer thin film on a soft polymer substrate for various applications.

ACKNOWLEDGMENTS

Authors would like to sincerely thank AFM Laboratory, Metallurgical and Materials Engineering, IIT Madras for providing nanoindentation facility for conducting all the experiments.

REFERENCES

1. Grove, N. R.; Kohl, P.; Bidstrup Allen, S. A.; Jayaraman, S.; Shick, R. *J. Polym. Sci. Part B: Polym. Phys.* **1999**, *37*, 3003.
2. Hölck, O.; Bauer, J.; Wittler, O.; Lang, K. D.; Michel, B.; Wunderle, B. Experimental contact Angle Determination and Characterisation of Interfacial Energies by Molecular Modelling of Chip to Epoxy Interfaces; I.E. 61st Electron. Compon. Technol. Confe. ECTC, S, **2011**, 1079.
3. Volinsky, A. A.; Moody, N. R.; Gerberich, W. W. Superlayer Residual Stress Effect on the Indentation Adhesion Measurements; Materials Research Society Symposium - Proceedings, Vol. *594* Materials Research Society, **2000**, 383.
4. Leterrier, Y.; Mottet, A.; Bouquet, N.; Gilliéron, D.; Dumont, P.; Pinyol, A. *Thin Solid Films* **2010**, *519*, 1729.
5. Vella, D.; Bico, J.; Boudaoud, A.; Roman, B.; Reis, P. M *Proc. Natl. Acad. Sci. U.S.A.* **2009**, *106*, 10901.
6. Ozmusul, M. S.; Picu, R. C. *Polym. Compos.* **2002**, *23*, 110.
7. Fang, X. Q.; Huang, M. J.; Liu, J. X.; Feng, W. J. *Compos. Sci. Technol.* **2014**, *98*, 79.
8. Fang, X. Q.; Zhang, L. L.; Liu, X. L.; Liu, J. X. *Appl. Math. Model* **2014**, *38*, 1041.
9. Wang, Z.; Volinsky, A.; Gallant, N. D. *J. Appl. Polym. Sci.* **2015**, *132*.
10. Mirsalehi, S. A.; Khavandi, A.; Mirdamadi, S.; Naimi-Jamal, M. R.; Kalantari, S. M. *J. Appl. Polym. Sci.* **2015**, *132*.
11. Li, M.; Carter, C. B.; Hillmyer, M.; Gerberich, W. W. *J. Mater. Res.* **2001**, *16*, 3378.
12. Sun, B.; Scherban, T. *Honolulu* **2013**, *2001*, 3. http://www.gruppofrattura.it/ocs/index.php/ICF/ICF10/paper/view/4531/6539.
13. Chang, S. Y.; Tsai, H. C.; Chang, J. Y.; Lin, S. J.; Chang, Y. S. *Thin Solid Films* **2008**, *516*, 5334.
14. Geng, K.; Yang, F.; Druffel, T.; Grulke, E. *Polymer (Guildf)* **2005**, *46*, 11768.
15. Zhang, T. Y.; Xu, W. H. *J. Mater. Res.* **2002**, *17*, 1715.
16. Chen, Z.; Diebels, S.; Peter, N. J.; Schneider, A. S. *Comput. Mater. Sci.* **2013**, *72*, 127.
17. Pelegri, A.; Huang, X. *Compos. Sci. Technol.* **2008**, *68*, 147.
18. Xu, Z. H.; Rowcliffe, D. *Thin Solid Films* **2004**, *447-448*, 399.
19. Antunes, J. M.; Fernandes, J. V.; Sakharova, N.; Oliveira, M. C.; Menezes, L. F. *Int. J. Solids Struct.* **2007**, *44*, 8313.
20. Pelletier, H.; Krier, J.; Mille, P. *Mech. Mater.* **2006**, *38*, 1182.
21. Kramer, D. E.; Volinsky, A.; Moody, N. R.; Gerberich, W. W. *J. Mater. Res.* **2001**, *16*, 3150.
22. Wang, M.; Liechti, K. M.; White, J. M.; Winter, R. M. *J. Mech. Phys. Solids* **2004**, *52*, 2329.
23. Mattei, G.; Gruca, G.; Rijnveld, N.; Ahluwalia, A. *J. Mech. Behav. Biomed. Mater.* **2015**, *50*, 150.
24. Zhou, J.; Komvopoulos, K. *J. Appl. Phys.* **2006**, *100*.
25. Koumoulos, E. P.; Charitidis, C.; Papageorgiou, D. P.; Papathanasiou, A. G.; Boudouvis, A. G. *Surf. Coat. Technol.* **2012**, *206*, 3823.
26. Volinsky, A.; Moody, N. R.; Gerberich, W. W. *Acta Mater.* **2002**, *50*, 441.
27. Barletta, M.; Bellisario, D.; Rubino, G.; Ucciardello, N. *Prog. Org. Coat.* **2010**, *68*, 100.
28. Barletta, M.; Lusvarghi, L.; Mantini, F. P.; Rubino, G. *Coat. Technol.* **2007**, *201*, 7479.
29. Barletta, M.; Gisario, A.; Lusvarghi, L.; Bolelli, G.; Rubino, G. *Appl. Surf. Sci.* **2008**, *254*, 7198.

30. Barletta, M.; Gisario, a.; Rubino, G.; Lusvarghi, L. *Prog. Org. Coat.* **2009**, *64*, 247.
31. Giro-paloma, J.; Rayón, E.; Roa, J. J.; Martínez, M.; Fernández, A. I. *Eur. Polym. J.* **2015**, *63*, 29.
32. Li, H.; Ngan, A. H. W. *J. Mater. Res.* **2004**, *19*, 513.
33. Zheng, X. J.; Zhou, Y. C. *Compos. Sci. Technol.* **2005**, *65*, 1382.
34. Huang, X.; Pelegri, A. *Compos. Sci. Technol.* **2007**, *67*, 1311.
35. Manual, T. U. HYSITRON (Revision 9.2.1211).
36. Leterrier, Y.; Waller, J.; Månson, J. A. E.; Nairn, J. *Mech. Mater.* **2010**, *42*, 326.
37. Li, T.; Huang, Z. Y.; Xi, Z. C.; Lacour, S. P.; Wagner, S.; Suo, Z. *Mech. Mater* **2005**, *37*, 261.
38. Oliver, W. C.; Pharr, G. M. *J. Mater. Res.* **2004**, *19*, 3.